Electronic Supplementary Material

Analysis of structural distortion in Eshelby twisted InP nanowires by scanning precession electron diffraction

Daniel Ugarte[1,2] (✉), Luiz H. G. Tizei[3], Monica A. Cotta[1], Caterina Ducati[2], Paul A. Midgley[2], and Alexander S. Eggeman[2,4] (✉)

[1] *CAS Center for Excellence in Nanoscience, CAS Key Laboratory for Biomedical Effects of Nanomaterials and Nanosafety, National Center for Nanoscience*
[1] *Instituto de Física "Gleb Wataghin", Universidade Estadual de Campinas-UNICAMP, CEP 13083-859, Campinas - SP, Brazil*
[2] *Department of Materials Science and Metallurgy, University of Cambridge, Cambridge CB3 0FS, UK*
[3] *Laboratoire de Physique des Solides, CNRS UMR8502, Univ. Paris Sud, 91405 Orsay, France*
[4] *School of Materials, University of Manchester, Manchester, M13 9PL, UK*

Supporting information to https://doi.org/10.1007/s12274-019-2328-5

This section contains:

a) Crystal structure of the wurtzite InP nanowires
b) Determination of nanowire width
c) Determination of the 3D curve followed by the NW axis.
d) Effect of the 3D shape of the wire on the image focusing
e) HSR-PED experiment with well oriented crystals.
f) Linear averaging of the misorientation along electron trajectory
g) Poison denoising of PED patterns by the Anscombe transformation
h) Video 1.
Dynamical animations of the HSR-PED data acquisition, where each video-frame includes: 1) the real space image of the wire and a spot indicating measurement position; 2) the PED pattern corresponding to the indicated pixel and finally,; 3) the pole figure of the crystal. This animation pictures a well oriented wire (wire axis perpendicular to electron beam)
i) Video 2.
Dynamical animations of the HSR-PED data acquisition, where each video-frame includes: 1) the real space image of the wire and a spot indicating measurement position; 2) the PED pattern corresponding to the indicated pixel and finally; 3) the pole figure of the crystal. This animation pictures a misoriented wire (wire axis about 10ºoff the plane perpendicular to electron beam)
a) Crystal structure of the Wurszite InP nanowires

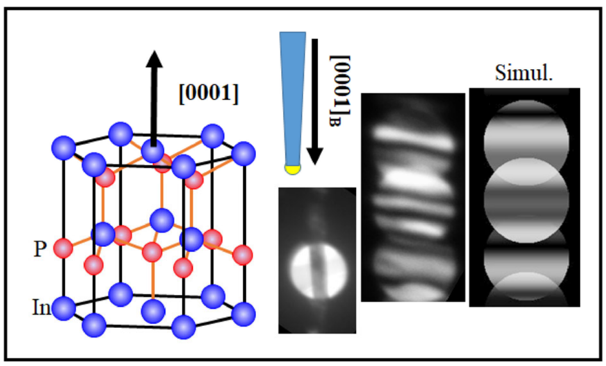

Figure S1 Crystal structure of the wurtzite InP nanowires grown by VLS in a CBE reactor. This InP hexagonal phase (6/mmm point group [24]) is not observed in macroscopic crystals; as expected due to symmetry considerations, the wire axis is parallel to the hexagonal [0001] direction (*c*-axis). The typical growth direction is $[0001]_B$, which is anion (P) terminated; this was confirmed by CBED measurements (displayed at right).

b) Determination of nanowire diameter
Given the sensitivity of the Eshelby twist to the size of the nanowire care was taken to ensure this value was accurately measured. Firstly regions of the nanowire were imaged using conventional ADF STEM (FEI Tecnai Osiris 80-200, 200 KeV) in the studied region (Figure SI2a); we must keep in mind that these long wires display a very slight tapering along their length. The average between wire diameters at both wire extrema (left- and right side intensity profiles) were used to estimate the wire width as (32±2) nm. Also, we must consider that the InP nanowires may present a thin oxide layer or amorphous carbon contamination deposited during the electron microscopy observation), then

Address correspondence to Daniel Ugarte, dmugarte@ifi.unicamp.br; Alexander Eggeman, alexander.eggeman@manchester.ac.uk

the actual crystalline core may be slightly less than the value deduced from ADF images. HSR-PED provides an additional means of estimating NW crystal core through PED quality fit factor (Fit-Q, Index parameter in ASTAR analysis). Figure SI2b compares the intensity profiles for VADF and fit quality factor values and as expected the Fit-Q profiles is lightly narrower. We have also looked at individual PED patterns and very weak crystal diffraction disks are observed for pixels in the region between 14-15 nm in radius, so considering the ensemble of available information, we have taken the NW radius as (15±1) nm for Eshelby twist theoretical estimation.

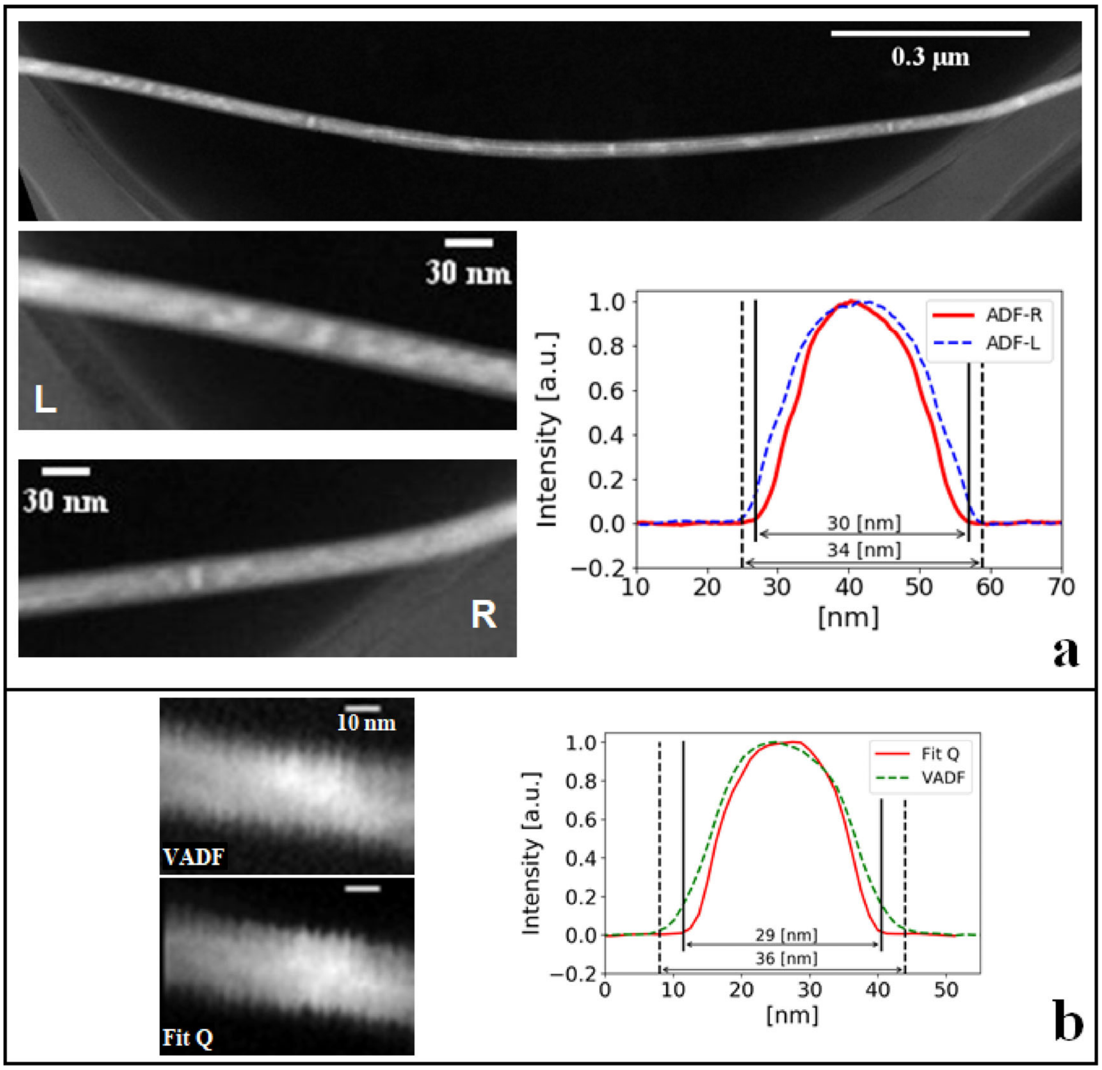

Figure S2 (a) Scanning transmission electron microscopy annular dark field (ADF) images of the studied thin InP nanowire (FEI Tecnai Osiris 80-200, 200 KeV; b) comparison of wire diameter estimation using VADF and Fit Quality profiles derived from HSR-PED data (0.5° precession angle, 1.25 nm/pixel).

c) Determination of the 3D curve followed by the NW axis.

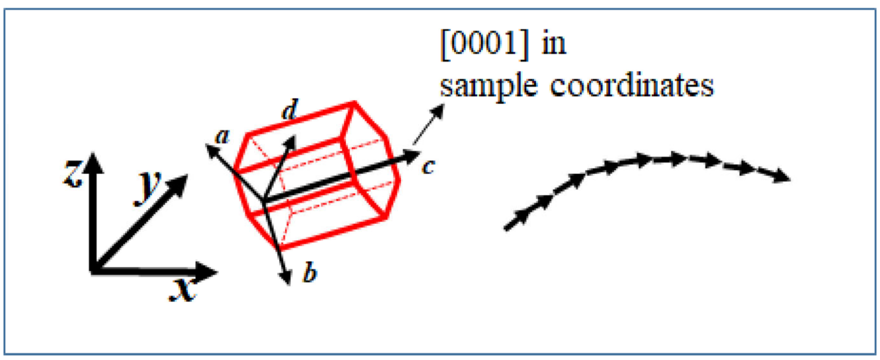

Figure S3 Schematic drawing showing the derivation of the 3D position of the nanowire geometrical axis by the addition pixel by pixel of the PED derived c-axis orientation in sample coordinates.

d) Effect of the 3D shape on the wire on the image focusing

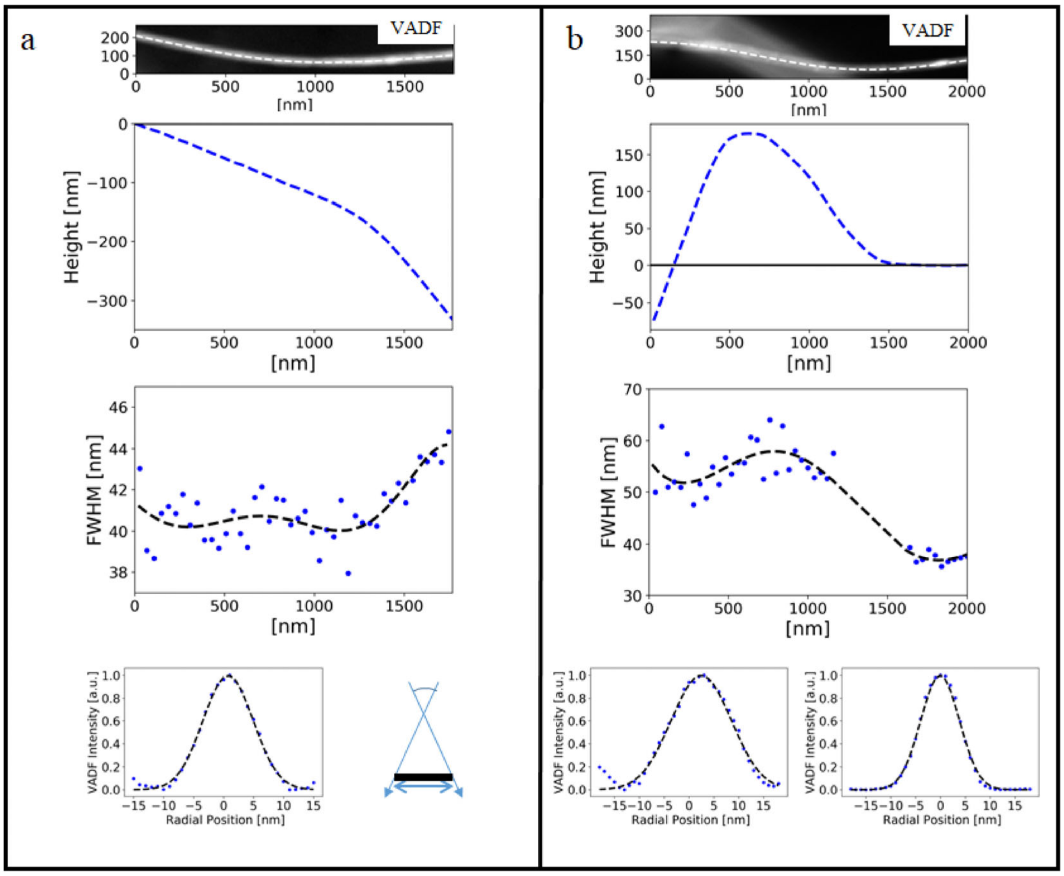

Figure S4 Use of HSR-PED to derive the 3D curvature of the InP nanowires. We display two different cases (a) and (b). For each case, we show in the top region a VADF image, the sample height, and the measure wire diameters. At the figure lower part we plot some examples of the Gaussian fits to the VADF intensity profiles. Also, lower part of (a) shows and schematic drawing of the effect of beam broadening due to sample height movement away from the pivot points.

e) HSR-PED experiment with well oriented crystals.

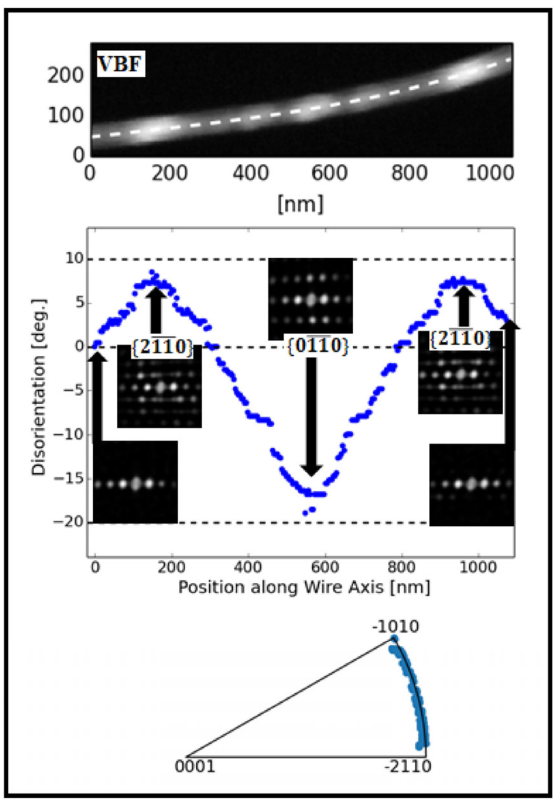

Figure S5 Disorientation map for a nanowire region whose axis is perpendicular to the electron beam (as indicated by the inverse pole figure displayed at the bottom of the figure). In contrast to Figure 4b, the disorientation curve is very noisy and it does not attain the expected values close to zone axes positions.

f) Linear averaging of the misorientation along electron trajectory

As shown in the schematic drawing at the right of Figure S6a, when a narrow electron beam travels through the wire, the distance to the wires axis changes continuously along the trajectory. Also, the disorientation of the *c*-axis depends on that distance, then we must average the *c*-axis deviation (essentially the normal component N_θ along the electron trajectory).

$$\langle N_{Screw}\rangle_x = \frac{1}{(2y_{max})}\int_{-y_{max}}^{y_{max}} N_\theta \sin(\theta)\,dy$$

$$\langle N_{Screw}\rangle_y = \frac{1}{(2y_{max})}\int_{-y_{max}}^{y_{max}} N_\theta \cos(\theta)\,dy$$

A quick analysis of Fig. S6a easily demonstrates that the in-plane component (perpendicular to the electron beam) cancels due to the opposite contribution of upper and bottom wire sectors. Then, due to the integration along the electron path the dislocation field will be just revealed though a wurtzite *c*-axis disorientation in a direction parallel to the electron trajectory. Fig. S6b show the predicted deviation of the *c*-axis due to helicoid arrangement of the basal plane due to the screw dislocation (thin lines 1/r dependence, thick continuous lines average along electron trajectory). This indicates a discrete jump of misorientation at the wire center, which is smoothed if the width of the electron probe is considered (dashed lines in Figure S6b).

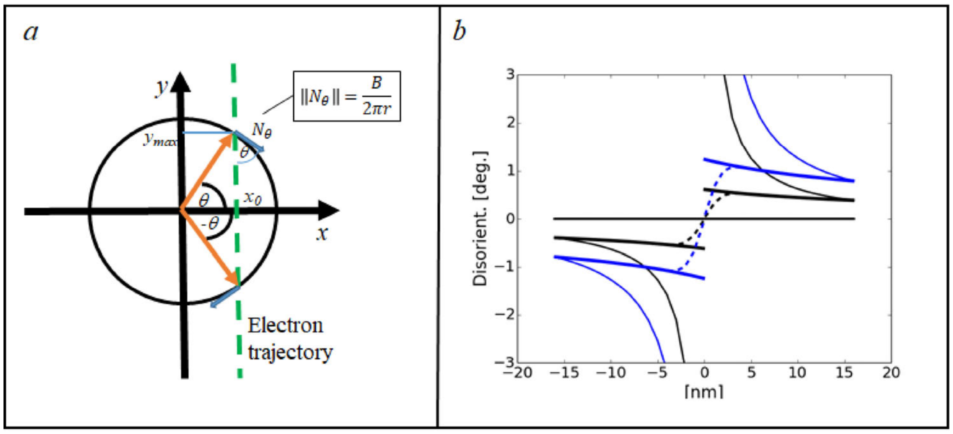

Figure S6 Simple model considering that the c-axis misorientation associated with the screw dislocation behaves as the average deviation along the electron trajectory. Thin line represent the angular deviation when the pure deformation field of a screw dislocation is considered (1/*r* dependence, black |***B***|= |***c***|, blue |***B***|= 2 |***c***|), thick line represent deviation averaged values. Dashed line represent the effect on misorientation measurement when the electron probe width (2.5 nm) is accounted for.

g) Poisson Denoising of PED patterns by the Anscombe transformation.

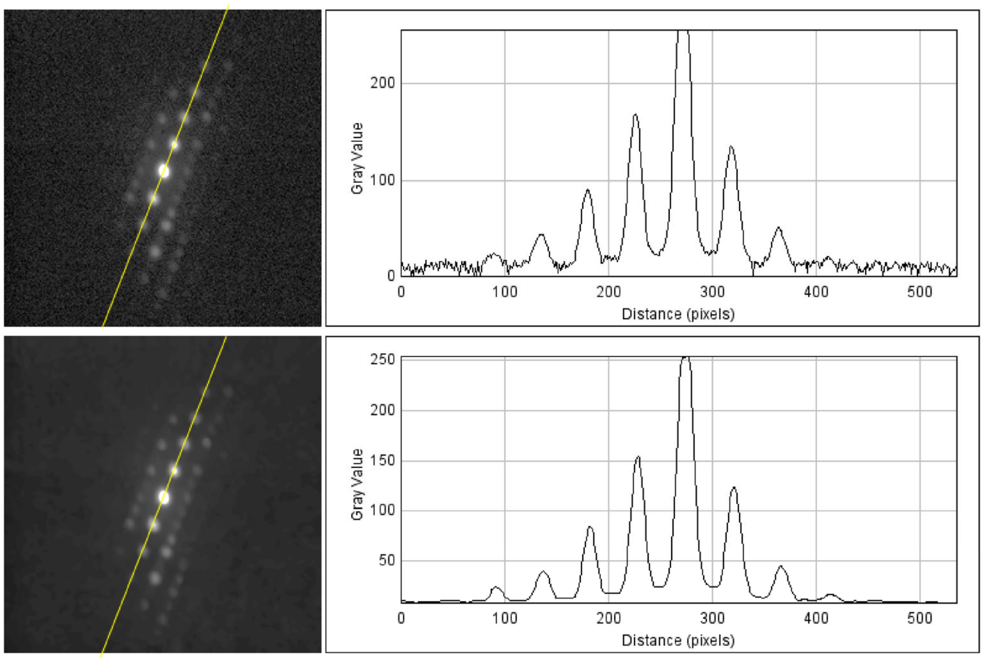

Figure S7 Effect of the denoising procedure based on the Anscombe transformation and collaborative denoising (BM3D) on PED diffraction patterns. Note that the visibility of high angle peaks is significantly increased.